Measurement of $e^+e^- \to K^+K^-$ cross section at $\sqrt{s} = 2.00 - 3.08$ GeV

M. Ablikim[1], M. N. Achasov[10,d], S. Ahmed[15], M. Albrecht[5], M. Alekseev[54A,54C], A. Amoroso[54A,54C], F. F. An[1], Q. An[41,51], J. Z. Bai[1], Y. Bai[40], O. Bakina[25], R. Baldini Ferroli[21A], Y. Ban[33], D. W. Bennett[20], J. V. Bennett[6], N. Berger[24], M. Bertani[21A], D. Bettoni[22A], F. Bianchi[54A,54C], E. Boger[25,b], I. Boyko[25], R. A. Briere[6], H. Cai[56], X. Cai[1,41], O. Cakir[44A], A. Calcaterra[21A], G. F. Cao[1,45], S. A. Cetin[44B], J. Chai[54C], J. F. Chang[1,41], G. Chelkov[25,b,c], G. Chen[1], H. S. Chen[1,45], J. C. Chen[1], M. L. Chen[1,41], S. J. Chen[31], X. R. Chen[28], Y. B. Chen[1,41], X. K. Chu[33], G. Cibinetto[22A], F. Cossio[54C], H. L. Dai[1,41], J. P. Dai[36,h], A. Dbeyssi[15], D. Dedovich[25], Z. Y. Deng[1], A. Denig[24], I. Denysenko[25], M. Destefanis[54A,54C], F. De Mori[54A,54C], Y. Ding[29], C. Dong[32], J. Dong[1,41], L. Y. Dong[1,45], M. Y. Dong[1], O. Dorjkhaidav[23], Z. L. Dou[31], S. X. Du[58], P. F. Duan[1], J. Fang[1,41], S. S. Fang[1,45], Y. Fang[1], R. Farinelli[22A,22B], L. Fava[54B,54C], S. Fegan[24], F. Feldbauer[5], G. Felici[21A], C. Q. Feng[41,51], E. Fioravanti[22A], M. Fritsch[5], C. D. Fu[1], Q. Gao[1], X. L. Gao[41,51], Y. Gao[43], Y. G. Gao[7], Z. Gao[41,51], B. Garillon[24], I. Garzia[22A], K. Goetzen[11], L. Gong[32], W. X. Gong[1,41], W. Gradl[24], M. Greco[54A,54C], M. H. Gu[1,41], S. Gu[16], Y. T. Gu[13], A. Q. Guo[1], R. P. Guo[1], Y. P. Guo[24], Z. Haddadi[27], S. Han[56], X. Q. Hao[16], F. A. Harris[46], K. L. He[1,45], X. Q. He[50], F. H. Heinsius[5], T. Held[5], Y. K. Heng[1], T. Holtmann[5], Z. L. Hou[1], H. M. Hu[1,45], J. F. Hu[36,h], T. Hu[1], Y. Hu[1], G. S. Huang[41,51], J. S. Huang[16], S. H. Huang[42], X. T. Huang[35], X. Z. Huang[31], Z. L. Huang[29], T. Hussain[53], W. Ikegami Andersson[55], Q. Ji[1], Q. P. Ji[16], X. B. Ji[1,45], X. L. Ji[1,41], X. S. Jiang[1], X. Y. Jiang[32], J. B. Jiao[35], Z. Jiao[18], D. P. Jin[1], S. Jin[1,45], Y. Jin[47], T. Johansson[55], A. Julin[48], N. Kalantar-Nayestanaki[27], X. S. Kang[32], M. Kavatsyuk[27], B. C. Ke[6], T. Khan[41,51], A. Khoukaz[49], P. Kiese[24], R. Kliemt[11], L. Koch[26], O. B. Kolcu[44B,f], B. Kopf[5], M. Kornicer[46], M. Kuemmel[5], M. Kuhlmann[5], A. Kupsc[55], W. Kühn[26], J. S. Lange[26], M. Lara[20], P. Larin[15], L. Lavezzi[54C,1], H. Leithoff[24], C. Leng[54C], C. Li[55], Cheng Li[41,51], D. M. Li[58], F. Li[1,41], F. Y. Li[33], G. Li[1], H. B. Li[1,45], H. J. Li[1], J. C. Li[1], Jin Li[34], K. J. Li[42], Kang Li[14], Ke Li[1], Lei Li[4], P. L. Li[41,51], P. R. Li[8,45], Q. Y. Li[35], W. D. Li[1,45], W. G. Li[1], X. L. Li[35], X. N. Li[1,41], X. Q. Li[32], Z. B. Li[42], H. Liang[41,51], Y. F. Liang[38], Y. T. Liang[26], G. R. Liao[12], J. Libby[2], D. X. Lin[15], B. Liu[36,h], B. J. Liu[1], C. X. Liu[1], D. Liu[41,51], F. H. Liu[37], Fang Liu[1], Feng Liu[7], H. B. Liu[13], H. M. Liu[1,45], Huanhuan Liu[1], Huihui Liu[17], J. B. Liu[41,51], J. Y. Liu[1], K. Liu[43], K. Y. Liu[29], Ke Liu[7], L. D. Liu[33], Q. Liu[45], S. B. Liu[41,51], X. Liu[28], Y. B. Liu[32], Z. A. Liu[1], Zhiqing Liu[24], Y. F. Long[33], X. C. Lou[1], H. J. Lu[18], J. G. Lu[1,41], Y. Lu[1], Y. P. Lu[1,41], C. L. Luo[30], M. X. Luo[57], X. L. Luo[1,41], X. R. Lyu[45], F. C. Ma[29], H. L. Ma[1], L. L. Ma[35], M. M. Ma[1], Q. M. Ma[1], T. Ma[1], X. N. Ma[32], X. Y. Ma[1,41], Y. M. Ma[35], F. E. Maas[15], M. Maggiora[54A,54C], Q. A. Malik[53], Y. J. Mao[33], Z. P. Mao[1], S. Marcello[54A,54C], Z. X. Meng[47], J. G. Messchendorp[27], G. Mezzadri[22B], J. Min[1,41], R. E. Mitchell[20], X. H. Mo[1], Y. J. Mo[7], C. Morales Morales[15], G. Morello[21A], N. Yu. Muchnoi[10,d], H. Muramatsu[48], A. Mustafa[5], Y. Nefedov[25], F. Nerling[11], I. B. Nikolaev[10,d], Z. Ning[1,41], S. Nisar[9], S. L. Niu[1,41], X. Y. Niu[1], S. L. Olsen[34], Q. Ouyang[1], S. Pacetti[21B], Y. Pan[41,51], M. Papenbrock[55], P. Patteri[21A], M. Pelizaeus[5], J. Pellegrino[54A,54C], H. P. Peng[41,51], K. Peters[11,g], J. Pettersson[55], J. L. Ping[30], R. G. Ping[1,45], A. Pitka[5], R. Poling[48], V. Prasad[41,51], H. R. Qi[3], M. Qi[31], T. .Y. Qi[3], S. Qian[1,41], C. F. Qiao[45], N. Qin[56], X. S. Qin[5], Z. H. Qin[1,41], J. F. Qiu[1], K. H. Rashid[53,i], C. F. Redmer[24], M. Richter[5], M. Ripka[24], M. Rolo[54C], G. Rong[1,45], Ch. Rosner[15], A. Sarantsev[25,e], M. Savrié[22B], C. Schnier[5], K. Schoenning[55], W. Shan[33], M. Shao[41,51], C. P. Shen[3], P. X. Shen[32], X. Y. Shen[1,45], H. Y. Sheng[1], J. J. Song[35], W. M. Song[35], X. Y. Song[1], S. Sosio[54A,54C], C. Sowa[5], S. Spataro[54A,54C], G. X. Sun[1], J. F. Sun[16], L. Sun[56], S. S. Sun[1,45], X. H. Sun[1], Y. J. Sun[41,51], Y K Sun[41,51], Y. Z. Sun[1], Z. J. Sun[1,41], Z. T. Sun[20], C. J. Tang[38], G. Y. Tang[1], X. Tang[1], I. Tapan[44C], M. Tiemens[27], B. T. Tsednee[23], I. Uman[44D], G. S. Varner[46], B. Wang[1], B. L. Wang[45], D. Wang[33], D. Y. Wang[33], Dan Wang[45], K. Wang[1,41], L. L. Wang[1], L. S. Wang[1], M. Wang[35], P. Wang[1], P. L. Wang[1], W. P. Wang[41,51], X. F. Wang[43], Y. Wang[39], Y. D. Wang[15], Y. F. Wang[1], Y. Q. Wang[24], Z. Wang[1,41], Z. G. Wang[1,41], Z. Y. Wang[1], Zongyuan Wang[1], T. Weber[5], D. H. Wei[12], J. H. Wei[32], P. Weidenkaff[24], S. P. Wen[1], U. Wiedner[5], M. Wolke[55], L. H. Wu[1], L. J. Wu[1], Z. Wu[1,41], L. Xia[41,51], Y. Xia[19], D. Xiao[1], Y. J. Xiao[1], Z. J. Xiao[30], X. H. Xie[42], Y. G. Xie[1,41], Y. H. Xie[7], X. A. Xiong[1], Q. L. Xiu[1,41], G. F. Xu[1], J. J. Xu[1], L. Xu[1], Q. J. Xu[14], Q. N. Xu[45], X. P. Xu[39], L. Yan[54A,54C], W. B. Yan[41,51], W. C. Yan[3], Y. H. Yan[19], H. J. Yang[36,h], H. X. Yang[1], L. Yang[56], Y. H. Yang[31], Y. X. Yang[12], M. Ye[1,41], M. H. Ye[8], J. H. Yin[1], Z. Y. You[42], B. X. Yu[1], C. X. Yu[32], J. S. Yu[28], C. Z. Yuan[1,45], Y. Yuan[1], A. Yuncu[44B,a], A. A. Zafar[53], Y. Zeng[19], Z. Zeng[41,51], B. X. Zhang[1], B. Y. Zhang[1,41], C. C. Zhang[1], D. H. Zhang[1], H. H. Zhang[42], H. Y. Zhang[1,41], J. Zhang[1], J. L. Zhang[1], J. Q. Zhang[5], J. W. Zhang[1], J. Y. Zhang[1], J. Z. Zhang[1,45], K. Zhang[1], L. Zhang[43], S. Q. Zhang[32], X. Y. Zhang[35], Y. H. Zhang[1,41], Y. T. Zhang[41,51], Yang Zhang[1], Yao Zhang[1], Yu Zhang[45], Z. H. Zhang[7], Z. P. Zhang[51], Z. Y. Zhang[56], G. Zhao[1], J. W. Zhao[1,41], J. Y. Zhao[1], J. Z. Zhao[1,41], Lei Zhao[41,51], Ling Zhao[1], M. G. Zhao[32], Q. Zhao[1], S. J. Zhao[58], T. C. Zhao[1], Y. B. Zhao[1,41], Z. G. Zhao[41,51], A. Zhemchugov[25,b], B. Zheng[15,52], J. P. Zheng[1,41], W. J. Zheng[35], Y. H. Zheng[45], B. Zhong[30], L. Zhou[1,41], X. Zhou[56], X. K. Zhou[41,51], X. R. Zhou[41,51], X. Y. Zhou[1], J. Zhu[42], K. Zhu[1], K. J. Zhu[1], S. Zhu[1], S. H. Zhu[50], X. L. Zhu[43], Y. C. Zhu[41,51], Y. S. Zhu[1,45], Z. A. Zhu[1,45], J. Zhuang[1,41], B. S. Zou[1], J. H. Zou[1]

(BESIII Collaboration)

[1] *Institute of High Energy Physics, Beijing 100049, People's Republic of China*
[2] *Indian Institute of Technology Madras, Indian Institute of Technology Madras IIT P.O., Chennai 600 036, India*
[3] *Beihang University, Beijing 100191, People's Republic of China*
[4] *Beijing Institute of Petrochemical Technology, Beijing 102617, People's Republic of China*
[5] *Bochum Ruhr-University, D-44780 Bochum, Germany*
[6] *Carnegie Mellon University, Pittsburgh, Pennsylvania 15213, USA*
[7] *Central China Normal University, Wuhan 430079, People's Republic of China*
[8] *China Center of Advanced Science and Technology, Beijing 100190, People's Republic of China*
[9] *COMSATS Institute of Information Technology, Lahore, Defence Road, Off Raiwind Road, 54000 Lahore, Pakistan*

[10] G.I. Budker Institute of Nuclear Physics SB RAS (BINP), Novosibirsk 630090, Russia
[11] GSI Helmholtzcentre for Heavy Ion Research GmbH, D-64291 Darmstadt, Germany
[12] Guangxi Normal University, Guilin 541004, People's Republic of China
[13] Guangxi University, Nanning 530004, People's Republic of China
[14] Hangzhou Normal University, Hangzhou 310036, People's Republic of China
[15] Helmholtz Institute Mainz, Johann-Joachim-Becher-Weg 45, D-55099 Mainz, Germany
[16] Henan Normal University, Xinxiang 453007, People's Republic of China
[17] Henan University of Science and Technology, Luoyang 471003, People's Republic of China
[18] Huangshan College, Huangshan 245000, People's Republic of China
[19] Hunan University, Changsha 410082, People's Republic of China
[20] Indiana University, Bloomington, Indiana 47405, USA
[21] (A)INFN Laboratori Nazionali di Frascati, I-00044, Frascati, Italy; (B)INFN and University of Perugia, I-06100, Perugia, Italy
[22] (A)INFN Sezione di Ferrara, I-44122, Ferrara, Italy; (B)University of Ferrara, I-44122, Ferrara, Italy
[23] Institute of Physics and Technology, Peace Ave. 54B, Ulaanbaatar 13330, Mongolia
[24] Johannes Gutenberg University of Mainz, Johann-Joachim-Becher-Weg 45, D-55099 Mainz, Germany
[25] Joint Institute for Nuclear Research, 141980 Dubna, Moscow region, Russia
[26] Justus-Liebig-Universitaet Giessen, II. Physikalisches Institut, Heinrich-Buff-Ring 16, D-35392 Giessen, Germany
[27] KVI-CART, University of Groningen, NL-9747 AA Groningen, The Netherlands
[28] Lanzhou University, Lanzhou 730000, People's Republic of China
[29] Liaoning University, Shenyang 110036, People's Republic of China
[30] Nanjing Normal University, Nanjing 210023, People's Republic of China
[31] Nanjing University, Nanjing 210093, People's Republic of China
[32] Nankai University, Tianjin 300071, People's Republic of China
[33] Peking University, Beijing 100871, People's Republic of China
[34] Seoul National University, Seoul, 151-747 Korea
[35] Shandong University, Jinan 250100, People's Republic of China
[36] Shanghai Jiao Tong University, Shanghai 200240, People's Republic of China
[37] Shanxi University, Taiyuan 030006, People's Republic of China
[38] Sichuan University, Chengdu 610064, People's Republic of China
[39] Soochow University, Suzhou 215006, People's Republic of China
[40] Southeast University, Nanjing 211100, People's Republic of China
[41] State Key Laboratory of Particle Detection and Electronics, Beijing 100049, Hefei 230026, People's Republic of China
[42] Sun Yat-Sen University, Guangzhou 510275, People's Republic of China
[43] Tsinghua University, Beijing 100084, People's Republic of China
[44] (A)Ankara University, 06100 Tandogan, Ankara, Turkey; (B)Istanbul Bilgi University, 34060 Eyup, Istanbul, Turkey; (C)Uludag University, 16059 Bursa, Turkey; (D)Near East University, Nicosia, North Cyprus, Mersin 10, Turkey
[45] University of Chinese Academy of Sciences, Beijing 100049, People's Republic of China
[46] University of Hawaii, Honolulu, Hawaii 96822, USA
[47] University of Jinan, Jinan 250022, People's Republic of China
[48] University of Minnesota, Minneapolis, Minnesota 55455, USA
[49] University of Muenster, Wilhelm-Klemm-Str. 9, 48149 Muenster, Germany
[50] University of Science and Technology Liaoning, Anshan 114051, People's Republic of China
[51] University of Science and Technology of China, Hefei 230026, People's Republic of China
[52] University of South China, Hengyang 421001, People's Republic of China
[53] University of the Punjab, Lahore-54590, Pakistan
[54] (A)University of Turin, I-10125, Turin, Italy; (B)University of Eastern Piedmont, I-15121, Alessandria, Italy; (C)INFN, I-10125, Turin, Italy
[55] Uppsala University, Box 516, SE-75120 Uppsala, Sweden
[56] Wuhan University, Wuhan 430072, People's Republic of China
[57] Zhejiang University, Hangzhou 310027, People's Republic of China
[58] Zhengzhou University, Zhengzhou 450001, People's Republic of China

[a] Also at Bogazici University, 34342 Istanbul, Turkey
[b] Also at the Moscow Institute of Physics and Technology, Moscow 141700, Russia
[c] Also at the Functional Electronics Laboratory, Tomsk State University, Tomsk, 634050, Russia
[d] Also at the Novosibirsk State University, Novosibirsk, 630090, Russia
[e] Also at the NRC "Kurchatov Institute", PNPI, 188300, Gatchina, Russia
[f] Also at Istanbul Arel University, 34295 Istanbul, Turkey
[g] Also at Goethe University Frankfurt, 60323 Frankfurt am Main, Germany
[h] Also at Key Laboratory for Particle Physics, Astrophysics and Cosmology, Ministry of Education; Shanghai Key Laboratory for Particle Physics and Cosmology; Institute of Nuclear and Particle Physics, Shanghai 200240, People's Republic of China
[i] Government College Women University, Sialkot - 51310. Punjab, Pakistan.

(Dated: October 28, 2017)

The cross sections of the $e^+e^- \to K^+K^-$ process are measured precisely at center-of-mass energies $\sqrt{s}$ from 2.00 to 3.08 GeV using data collected with the BESIII detector operating at the Beijing Electron Positron Collider (BEPCII). The results are consistent with the previous measurements but with better precision. A resonant structure around 2.2 GeV is observed in the cross section line shape. A fit to the line shape yields a mass of $m = 2245.6 \pm 8.3 \pm 10.8$ MeV/c^2 and a width of $\Gamma = 136.3 \pm 11.8 \pm 9.2$ MeV, where the first uncertainty is statistical and the second is systematic. In addition, the kaon form factors are extracted from the cross sections.

PACS numbers: 13.60.Le, 13.40.Gp, 13.66.Jn, 14.40.Df

I. INTRODUCTION

With the observation of new structures in the $\phi - \psi$ region [1–4], it is of great interest to know if they are excited states of ρ, ω, ϕ or possible exotic particles, e.g. glueballs, hybrid mesons [5] or others. The identification of these particles requires better understanding of their decay patterns which can be investigated with exclusive processes in e^+e^- annihilations [6]. The knowledge of the $e^+e^- \to K^+K^-$ process can reveal properties of ρ, ω, ϕ and their excited states, e.g. $\phi(2170)$ is predicted to decay to kaon pairs according to the model in Ref. [7]. The form factor of the light mesons is also interesting and helps to understand the internal dynamics of hadrons, the detailed structure of hadronic wavefunctions, and the nuclear and hypernuclear forces [8, 9]. Furthermore, the asymptotic QCD can also be tested from the measurement of the kaon form factor at high energies, where the form factor F_K is predicted to be inversely proportional to the square of s.

Many efforts have been deployed to understand the $e^+e^- \to K^+K^-$ process [10–16]. In the energy region around the $\phi(1020)$ resonance, the uncertainties of the previous measured cross sections are of a few percent, while they are more than 15% for energies higher than 2.0 GeV. The *BABAR* experiment used initial-state radiation (ISR) technique to measure the $e^+e^- \to K^+K^-$ process in a wide energy range from the threshold of K^+K^- to 8 GeV and observed complicated structures between 1.8 and 2.4 GeV [12, 13]. In this paper, the $e^+e^- \to K^+K^-$ process has been studied with the energy scan method at 22 energies from 2.00 to 3.08 GeV. The uncertainties of the cross section measurement and the kaon form factor are reduced significantly.

II. DETECTOR AND DATA SAMPLES

BEPCII [17, 18] is a double-ring e^+e^- collider designed to provide a peak luminosity of 10^{33} cm^{-2}s^{-1} at $\sqrt{s} = 3.770$ GeV. The BESIII [17, 19] detector has a geometrical acceptance of 93% of the full solid angle and has four main components: (1) A small-cell, helium-based (60% He, 40% C_3H_8) main drift chamber (MDC) with 43 layers providing an average single-hit resolution of 135 μm, and a momentum resolution in a 1 T magnetic field of 0.5% at 1 GeV/c; (2) An electromagnetic calorimeter (EMC) in a cylindrical structure consisting of one barrel and two endcaps. The energy resolution for tracks with 1.0 GeV/c momentum is 2.5% (5%) in the barrel (endcaps), and the position resolution is 6 mm (9 mm), respectively; (3) A time of flight system is used for particle identification. It is composed of 5-cm-thick plastic scintillators, with 176 detectors of 2.4 m length in two layers in the barrel and 96 fan-shaped detectors in the endcaps. The barrel (endcaps) time resolution of 80 ps (110 ps) provides $2\sigma K/\pi$ separation for momenta up to 1.0 GeV/c; (4) The muon system (MUC) consists of 1272 m^2 of resistive plate chambers (RPCs) in nine barrel and eight endcap layers and provides 2 cm position resolution.

The data samples used in this analysis correspond to a total integrated luminosity of 651 pb^{-1}, collected at 22 center-of-mass (c.m.) energies between 2.00 and 3.08 GeV.

Monte Carlo (MC)-simulated signal and background samples are used to optimize the event selection criteria, estimate the background contamination and evaluate the selection efficiencies. The MC samples are generated using a GEANT4-based [20] simulation software package BESIII OBJECT ORIENTED SIMULATION TOOL [21], which includes the description of geometry and material, the detector response and the digitization model, as well as a database of the detector running conditions and performance.

In this analysis, the generator software package CONEXC [22] is used to simulate the signal MC samples $e^+e^- \to K^+K^-$, and calculate the corresponding correction for higher-order processes with one radiative photon in the final states. Simulated samples of the QED background processes $e^+e^- \to e^+e^-$, $\mu^+\mu^-$ and $\gamma\gamma$ are generated with the generator BABAYAGA [23]. The other background of the $e^+e^- \to$ hadrons and the $e^+e^- \to e^+e^-X$ (X can be hadrons or leptons) processes are generated with the generators LUARLW [24] and BESTWOGAM [25], respectively.

III. EVENT SELECTION

The signal events are required to have two good oppositely charged tracks, which are reconstructed with the hit information from the MDC. A good charged track must be within the MDC coverage, $|\cos\theta| < 0.93$, and is required to pass within 1 cm of the e^+e^- interaction point in the plane perpendicular to the beam and within ± 10 cm in the direction along the beam. To suppress the $e^+e^- \to (\gamma)e^+e^-$ background, two selection criteria are required. Firstly, the ratio E/p of each kaon candidate is required to be smaller than a certain value to maximize the signal to background ratio, where E and p are the energy deposited in the EMC and the momentum measured in the MDC, respectively. Secondly, the event should satisfy $\cos\theta_+ < 0.8$ for the positive track and $\cos\theta_- > -0.8$ for the negative track. To suppress multi-body processes, the opening angle between the two tracks in the e^+e^- c.m. system is required to be larger than 179°. The background from cosmic rays is rejected by requiring the difference of TOF recorded time between the two tracks to be less than 3 ns. Figure 1 and 2 show comparisons of the angular distributions between experimental data and MC simulation at $\sqrt{s} = 2.6444$ GeV. There is good agreement between data and MC simulations.

The momenta of the $K^\pm$ tracks are expected to be $p_{\rm exp} = \sqrt{s/4 - m_K^2}$, which allows to effectively distinguish the signal from other two-body processes. Figure 3 shows the scatter plot of momentum distribution of the two tracks after performing all selection criteria described above.

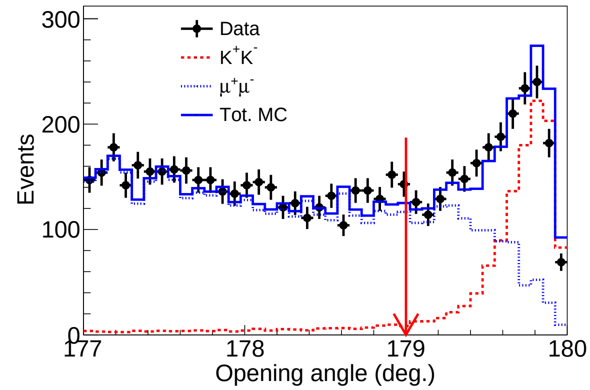

FIG. 2. Opening angle between the positive and the negative tracks at $\sqrt{s} = 2.6444$ GeV after performing all selection criteria, as well as a requirement that the momenta of the negative track should be within $3\sigma_p$ region of the signal. The arrow shows the selection requirement on the opening angle.

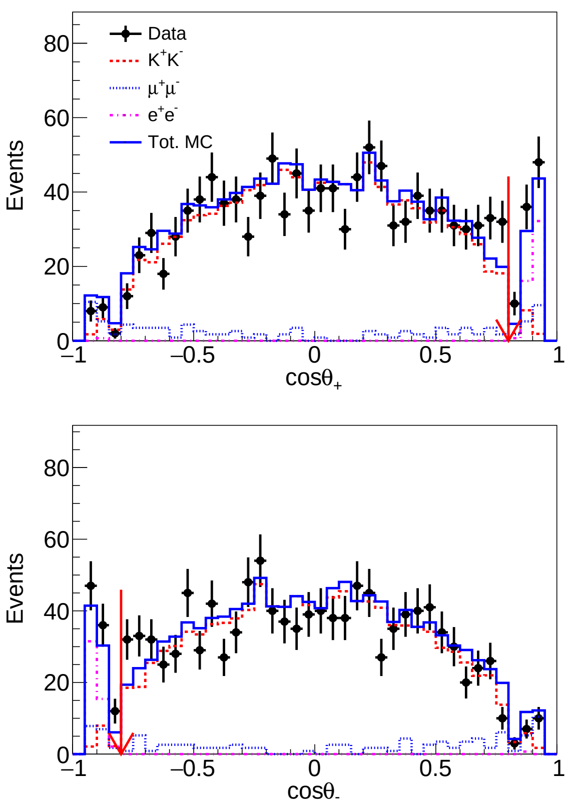

FIG. 1. Polar angular distribution of positive (upper) and negative (lower) tracks at 2.6444 GeV after performing all selection criteria, as well as a requirement that the momenta of both tracks should be within $3\sigma_p$ region of the signal, where is σ_p is the momentum resolution. The arrows show the selection requirements on the polar angular distribution of the tracks to suppress $e^+e^- \to (\gamma)e^+e^-$ background. "MC sum" in the legend means the sum of signal, $e^+e^- \to (\gamma)\mu^+\mu^-$ and $e^+e^- \to (\gamma)e^+e^-$ MC.

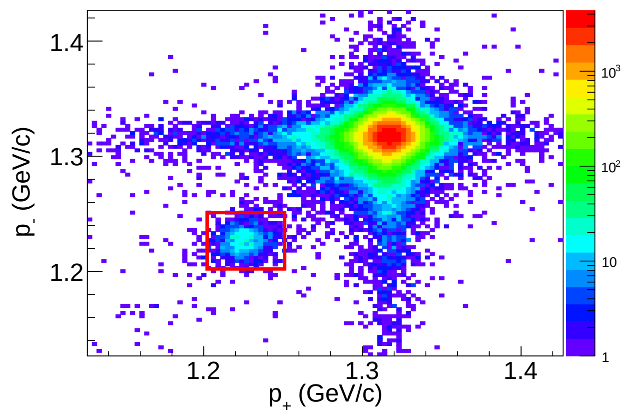

FIG. 3. Scatter plot of the momentum distribution of the positive (p_+) and the negative (p_-) track at $\sqrt{s} = 2.6444$ GeV. The signal events ($3\sigma_p$ region as shown in box) are concentrated around $p_{\rm exp} = 1.23$ GeV/c.

IV. BACKGROUND ANALYSIS

The potential background may come from hadronic processes with multi-body final states, or the e^+e^- annihilation processes with two-body final states, e.g. e^+e^-, $\mu^+\mu^-$ and $\pi^+\pi^-$, where a radiative process can reduce the momenta of final particles to the momentum region of kaon. The contamination of the background is evaluated by MC simulations in $3\sigma_p$ momentum region of the signal, where σ_p is the momentum resolution determined with signal MC. After imposing the above selection criteria, no events survived in $e^+e^- \to (\gamma)e^+e^-$, $\gamma\gamma$, and e^+e^-X processes. The background in hadronic final states is few and can be neglected. The dominant background comes from $e^+e^- \to (\gamma)\mu^+\mu^-$ and the normalized number of events in this process is summarized in Table I. The background level, defined as the ratio of the number of the background events to that of the signal, varies from 0.5% to 60% in dependence of c.m. energies and no peaks are observed in the signal region from background processes.

V. CROSS SECTION AND FORM FACTOR

A. Signal extraction

The number of signals is extracted by fitting the momentum spectrum of the positive track while the momentum of the negative track is required to be within $(p_{\rm exp} - 3\sigma_p, p_{\rm exp} + 3\sigma_p)$. In the fit, the signal is described by the signal MC shape convoluted with a Gaussian function and background is described with the MC shape of the $e^+e^- \to (\gamma)\mu^+\mu^-$ process convoluted with another Gaussian function. The convoluted Gaussian functions are supposed to composite the possible resolution deviation between data and MC simulation. Figure 4 illustrates the fit result at $\sqrt{s} = 2.6444$ GeV.

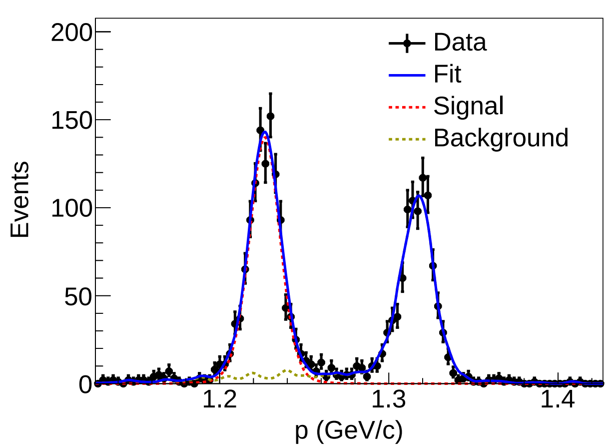

FIG. 4. Momentum spectrum at $\sqrt{s} = 2.6444$ GeV. Solid line represents the total fit function. Dash lines are signal (main part of left peak) and background (right peak and its tail).

B. Efficiency and correction factor

The Born cross section is calculated from

$$\sigma^B = \frac{N_{\rm sig}}{\mathcal{L}\cdot\epsilon\cdot(1+\delta)}, \tag{1}$$

where $N_{\rm sig}$ is the number of signal events, $\mathcal{L}$ is the integrated luminosity measured with method mentioned in [26], ϵ is the detection efficiency, $1+\delta$ is the correction factor due to ISR and vacuum polarization (VP).

The detection efficiency and the correction factor are obtained from the signal MC generated at each energy. In the generator, the cross section for ISR process ($\sigma_{e^+e^-\to\gamma X_i}$) is determined with the relation [22]

$$\sigma_{e^+e^-\to\gamma X_i} = \int d\sqrt{s'}\frac{2\sqrt{s'}}{s}W(s,x)\frac{\sigma^B(s')}{[1-\Pi(s')]^2}, \tag{2}$$

where $\sqrt{s'}$ is the effective c.m. energy of final states with $s' = s(1-x)$, and $x \equiv 2E_\gamma/\sqrt{s}$ with E_γ representing the energy of the radiated photon, $\Pi(s')$ represents the VP effect, which includes contributions from leptons and quarks, and $W(s,x)$ is the radiator function. To obtain a reliable detection efficiency ϵ and correction factor $1+\delta$, an iterative procedure is performed. Firstly, the *BABAR*'s cross sections are used as an initial line shape to generate signal MC. Then the calculated Born cross sections in this analysis with *BABAR*'s result are fitted with a phenomenological function, which is used as the input line shape. The procedure is repeated until the difference between last two iterations is less than 0.5%, thereby the iterative procedure is regarded as converged.- To obtain a reliable detection efficiency ϵ and correction factor $1+\delta$, an iterative procedure is performed.

For energies near the J/ψ resonance, the $J/\psi \to K^+K^-$ and the $e^+e^- \to K^+K^-$ processes interfere with each other. To correct the contribution from J/ψ decay and the interference, we use another data sample collected for J/ψ resonance study to extract the correction factor. In the extraction, we use a function containing amplitudes of the J/ψ decay and the continuum contribution to fit the line shape of the K^+K^- cross section and take the ratio of continuum contribution and total cross section as the correction factor. The Born cross sections and related variables are summarized in Table I.

C. Line shape of $e^+e^- \to K^+K^-$

The measured Born cross sections shown in Fig. 5 are consistent with that of the *BABAR* experiment but with better precision. The line shape of cross sections is fitted with [12, 27]

$$\sigma^B = |A_K|^2, \tag{3}$$

where the amplitude is written as

$$\begin{aligned} A_K = & c_\phi BW_\phi + c_{\phi'}BW_{\phi'} + c_{R1}BW_{R1} \\ & + c_\rho BW_\rho + c_{\rho'}BW_{\rho'} + c_{\rho''}BW_{\rho''} + c_{R2}BW_{R2} \\ & + c_\omega BW_\omega + c_{\omega'}BW_{\omega'} + c_{\omega''}BW_{\omega''} + c_{R3}BW_{R3} \\ & + c_{con}\cdot s^{-\alpha}\cdot e^{i\cdot\theta}, \end{aligned} \tag{4}$$

where c's are coefficients of resonances, including $\phi = \phi(1020)$, $\phi' = \phi(1680)$, $\rho = \rho(770)$, $\rho' = \rho(1450)$, $\rho'' = \rho(1700)$, $\omega = \omega(782)$, $\omega' = \omega(1420)$, $\omega'' = \omega(1650)$ and other resonances whose parameters are to be determined due to the lack of corresponding states in PDG, $R1$ denotes the structure around 2.23 GeV, while $R2$ and $R3$ are introduced to compensate some unknown contribution to the line shape. $s^{-\alpha}$ is used to describe the continuum process, θ is the relative phase between resonances and continuum process, BWs are Breit-Wigner functions of resonances, which take the form

$$BW(s, m, \Gamma(s)) = \frac{1}{m^2 - s - i\sqrt{s}\Gamma(s)}, \tag{5}$$

where m is the mass of resonances. The width $\Gamma(s)$ of a resonance is energy dependent. For the ρ resonance, energy dependence is given by

$$\Gamma_\rho(s) = \Gamma_\rho \frac{s}{m_\rho^2} \left(\frac{\beta(s, m_\pi)}{\beta(m_\rho^2, m_\pi)} \right)^3 \tag{6}$$

with $\beta(s, m) = \sqrt{1 - 4m^2/s}$. For the ϕ resonance, there are separate contributions from different decay modes, thereby the total width is parameterized in an approximate way as

$$\begin{aligned} \Gamma_\phi(s) =& \Gamma_\phi \Big[\mathcal{B}(\phi \to K^+K^-) \frac{\Gamma_{\phi\to K^+K^-}(s)}{\Gamma_{\phi\to K^+K^-}(m_\phi^2)} \\ &+ \mathcal{B}(\phi \to K^0\bar{K}^0) \frac{\Gamma_{\phi\to K^0\bar{K}^0}(s)}{\Gamma_{\phi\to K^0\bar{K}^0}(m_\phi^2)} \\ &+ 1 - \mathcal{B}(\phi \to K^+K^-) - \mathcal{B}(\phi \to K^0\bar{K}^0) \Big], \end{aligned} \tag{7}$$

where $\Gamma_{\phi\to K\bar{K}}(s)$ is similar to Eq. (6) but with ρ replaced by ϕ and π replaced by K, respectively, $\mathcal{B}$ is the Branching fraction. Fixed widths are used for resonances other than ϕ and ρ.

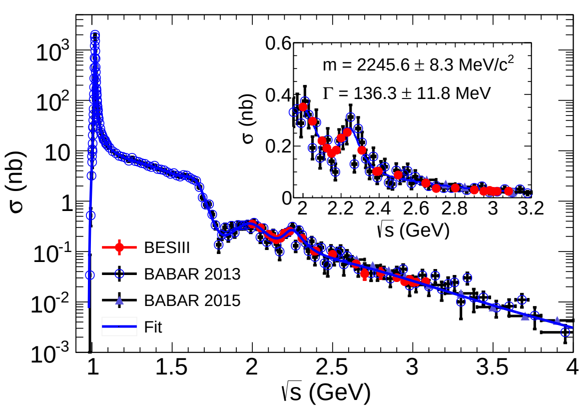

FIG. 5. Born cross section of the $e^+e^- \to K^+K^-$ process. Soft dots (in blue) and triangles with error bar are results of *BABAR*. Solid dots (in red) are results of BESIII (this work). The error bars include both statistical and systematic uncertainties. The fit is performed on both data from BESIII and *BABAR* using Eq. (3).

Masses and widths of (ϕ, ϕ'), (ρ, ρ', ρ'') and (ω, ω', ω'') are set to the values from Particle Data Group (PDG) [1], while masses and widths of ϕ'', ρ''' and ω''' are free. Parameters of resonances are determined from the *BABAR*'s cross sections below 2.00 GeV and from both the *BABAR*'s and the BESIII's measurement between 2.00 and 3.08 GeV . In the fit, statistical and systematic uncertainties are taken into consideration. For the BESIII's cross sections, systematic uncertainties from the ISR and the VP, the luminosity and the tracking efficiency are supposed as correlated while other uncertainties are treated as uncorrelated. The uncertainties of *BABAR*'s cross section are simply treated as uncorrelated. A structure with $m = 2245.6 \pm 8.3$ MeV/c^2 and $\Gamma = 136.3 \pm 11.8$ MeV is observed, as shown in Fig. 5. The amplitude of the resonance is not easy to extract because it is hard to determine the interference among several uncertain resonances used here.

D. Form factor

Experimentally, the form factor of charged kaon can be calculated from the cross section using following formula [12]

$$|F_K|^2(s) = \frac{3s}{\pi\alpha(0)^2\beta_K^3} \frac{\sigma^D}{C_{\rm FS}}, \tag{8}$$

where

$$\sigma^D = \sigma^B \left(\frac{\alpha(s)}{\alpha(0)} \right)^2 \tag{9}$$

is the dressed cross section, derived from the Born cross section σ^B, $\alpha(s)$ is the electromagnetic coupling constant, $\beta_K = \sqrt{1 - 4m_K^2/s}$ is the kaon velocity, and $C_{\rm FS}$ is the final-state correction [29–31]. The form factors can be found in Table I.

The asymptotic QCD predicts that the form factor of a spin zero meson is $F_K = 16\pi\alpha_s(s) f_K^2/s$ [28], where $\alpha_s(s)$ is the strong coupling constant and f_K is the weak decay amplitude of charged kaon. A fit to $|F_K|^2$ is performed with a function $A\alpha_s^2(s)/s^n$ at $\sqrt{s} > 2.38$GeV. A and n are allowed to vary in the fit as shown in Fig. 6. It is obtained that $n = 1.94 \pm 0.09$ which is in agreement with the QCD prediction $n = 2$. The fit is not implemented at lower energy range because there are resonances which can not be described by the function.

VI. SYSTEMATIC UNCERTAINTY

Several sources of systematic uncertainties are considered in the measurement of the Born cross section and the corresponding form factors, including those of the detection efficiency, the luminosity, the ISR and VP correction

TABLE I. Cross sections of $e^+e^- \to K^+K^-$ process and form factors of kaon. $N_{\rm sig}$ is the number of signal events, excluding the number of survived $\mu^+\mu^-$ events $N_{\mu\mu}^{\rm MC}$ in the signal region estimated from MC simulation, along with detection efficiency ϵ, radiative correction factor $1+\delta$, and luminosity $\mathcal{L}$. σ^B is the measured Born cross section, form which the form factor F_K is extracted. The first uncertainties are statistical and the second ones systematic. Uncertainties of form factor are propergated from those of cross sections.

$\sqrt{s}$ (GeV)	ϵ	$1+\delta$	$\mathcal{L}$ (pb^{-1})	$N_{\rm sig}$	$N_{\mu\mu}^{\rm MC}$	σ^B (pb)	$\|F_K\|^2$
2.0000	0.1927	2.717	10.074	1853.8 $\pm$ 43.3	9	351.5 $\pm$ 8.2 $\pm$ 6.4	0.1021 $\pm$ 0.0024 $\pm$ 0.0018
2.0500	0.1853	2.864	3.343	525.4 $\pm$ 23.2	3	296.1 $\pm$ 13.1 $\pm$ 4.7	0.0878 $\pm$ 0.0039 $\pm$ 0.0013
2.1000	0.1591	3.368	12.167	1438.0 $\pm$ 38.3	15	220.6 $\pm$ 5.9 $\pm$ 3.2	0.0666 $\pm$ 0.0018 $\pm$ 0.0009
2.1250	0.1453	3.704	108.49	11209.5$\pm$ 106.9	125	192.0 $\pm$ 1.8 $\pm$ 2.9	0.0593 $\pm$ 0.0006 $\pm$ 0.0009
2.1500	0.1346	3.987	2.841	261.7 $\pm$ 16.3	3	171.7 $\pm$ 10.7 $\pm$ 2.7	0.0539 $\pm$ 0.0034 $\pm$ 0.0008
2.1750	0.1521	3.521	10.625	1048.1 $\pm$ 32.7	12	184.2 $\pm$ 5.7 $\pm$ 3.0	0.0590 $\pm$ 0.0018 $\pm$ 0.0009
2.2000	0.1802	2.986	13.699	1706.0 $\pm$ 41.7	24	231.4 $\pm$ 5.7 $\pm$ 4.0	0.0744 $\pm$ 0.0018 $\pm$ 0.0013
2.2324	0.2011	2.707	11.856	1634.2 $\pm$ 40.8	17	253.2 $\pm$ 6.3 $\pm$ 4.2	0.0843 $\pm$ 0.0021 $\pm$ 0.0013
2.3094	0.1697	3.255	21.089	2143.3 $\pm$ 46.9	34	184.0 $\pm$ 4.0 $\pm$ 3.1	0.0635 $\pm$ 0.0014 $\pm$ 0.0010
2.3864	0.1222	4.557	22.549	1274.9 $\pm$ 36.4	40	101.5 $\pm$ 2.9 $\pm$ 2.1	0.0367 $\pm$ 0.0010 $\pm$ 0.0007
2.3960	0.1189	4.702	66.869	3837.3 $\pm$ 63.2	148	102.6 $\pm$ 1.7 $\pm$ 2.2	0.0371 $\pm$ 0.0006 $\pm$ 0.0008
2.5000	0.1005	5.616	1.098	54.6 $\pm$ 7.6	2	88.1 $\pm$ 12.2 $\pm$ 2.8	0.0341 $\pm$ 0.0047 $\pm$ 0.0011
2.6444	0.0909	6.289	33.722	1091.9 $\pm$ 34.7	110	56.6 $\pm$ 1.8 $\pm$ 2.1	0.0237 $\pm$ 0.0008 $\pm$ 0.0009
2.6464	0.0902	6.300	34.003	1095.3 $\pm$ 34.9	100	56.7 $\pm$ 1.8 $\pm$ 1.6	0.0240 $\pm$ 0.0008 $\pm$ 0.0006
2.7000	0.0873	6.580	1.034	21.6 $\pm$ 5.0	3	36.3 $\pm$ 8.4 $\pm$ 1.2	0.0158 $\pm$ 0.0037 $\pm$ 0.0005
2.8000	0.0804	7.159	1.008	22.1 $\pm$ 5.1	4	37.9 $\pm$ 8.8 $\pm$ 1.6	0.0173 $\pm$ 0.0040 $\pm$ 0.0007
2.9000	0.0738	7.837	105.253	1847.8 $\pm$ 48.1	496	30.4 $\pm$ 0.8 $\pm$ 1.4	0.0145 $\pm$ 0.0004 $\pm$ 0.0007
2.9500	0.0702	8.217	15.942	232.9 $\pm$ 17.3	87	25.3 $\pm$ 1.9 $\pm$ 1.3	0.0125 $\pm$ 0.0009 $\pm$ 0.0006
2.9810	0.0683	8.466	16.071	260.6 $\pm$ 15.1	87	28.0 $\pm$ 1.6 $\pm$ 1.6	0.0139 $\pm$ 0.0008 $\pm$ 0.0008
3.0000	0.0667	8.622	15.881	215.5 $\pm$ 16.9	90	24.4 $\pm$ 1.8 $\pm$ 1.5	0.0122 $\pm$ 0.0009 $\pm$ 0.0007
3.0200	0.0656	8.791	17.290	235.9 $\pm$ 18.2	99	24.8 $\pm$ 1.8 $\pm$ 1.5	0.0124 $\pm$ 0.0009 $\pm$ 0.0008
3.0800	0.0564	9.266	126.185	1335.6 $\pm$ 44.0	864	25.3 $\pm$ 0.7 $\pm$ 2.2	0.0118 $\pm$ 0.0003 $\pm$ 0.0010

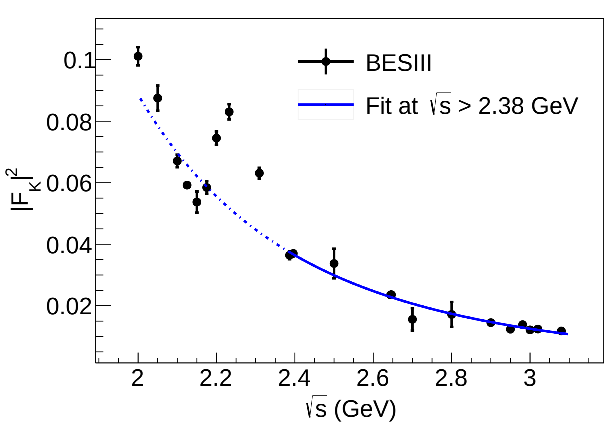

FIG. 6. $|F_K|^2$ of $e^+e^- \to K^+K^-$. Dots (in black) are results in this work. Solid Line (in blue) is the fit result at $\sqrt{s} > 2.38$ GeV while dotted line is extrapolation of solid line to show the trend of pQCD prediction at lower energy.

factor, background shape, and signal shape. The uncertainty sources for the detection efficiency include systematic uncertainties in tracking efficiency, the p and E/p requirements, opening angle between the positive and the negative tracks, and the MC statistics. The uncertainty of tracking efficiency is investigated using a control sample $e^+e^- \to K^+K^-\pi^+\pi^-$ with the strategy described in Ref [32]. Kaons have momenta that range from 0.85 to 1.45 GeV/c, and their transverse-momentum-weighted tracking efficiency is about 1% per track. For the p, E/p and opening angle requirements, the distributions of corresponding variables in MC simulation are smeared to those in data and the differences of cross sections under the same requirements are taken as the systematic uncertainties. The uncertainty of MC statistics is estimated by $\Delta_{MC} = \frac{1}{\sqrt{N}} \cdot \sqrt{\frac{1-\epsilon}{\epsilon}}$, where N is the number of signal MC events. The integrated luminosities are measured using large angle Bhabha scattering events, with an uncertainty of about 1% [26]. In the ISR and VP correction procedure, the cross section measurement is iterated until $(1+\delta)\epsilon$ converges. The difference between last two iterations is taken as the systematic uncertainty. Uncertainties due to the choice of the signal shape and background shapes, and the fit range are estimated by changing signal and background functions, and the fit range, respectively. All systematic uncertainties of cross section measurement are summarized in Table II.

The systematic uncertainties in the resonance parameters come from the absolute c.m. energy measurement, the systematic uncertainty on the cross section measurement, and the model used to describe the resonance. The uncertainty of c.m. energy provided by BEPCII is small and negligible in the extraction of the resonance parameters. The systematic uncertainty of the cross section measurement has already been considered in the fit of the cross section line shape. To assess the systematic uncertainty connected with the model, a modified Breit-Wigner function, considering the vertex function and phase space factor, is used to describe the resonance. The systematic uncertainties of the mass and the width are 6.2 MeV/c^2 and 0.9 MeV, respectively. The width the resonance is quite large, which may be energy-dependent. If we parameterized the width to be similar with Γ_ρ, this will introduce an uncertainty of 3.6 MeV/c^2 and 5.4 MeV for mass and width, respectively. Besides the Breit-Wigner function, the model is based on a sum of several resonances and parameters for some of them are quoted from PDG. The uncertainties due to the quoted parameters are estimated by sampling the parameters for many times according to their masses and uncertainties in PDG with Gaussian assumption. The systematic uncertainties are estimated to be 8.8 MeV/c^2 and 9.2 MeV for mass and width, respectively. The overall systematic uncertainties are obtained by summing all independent uncertainties in quadrature, which are 11.4 MeV/c^2 for mass and 10.7 MeV for width

VII. CONCLUSION

In summary, we measure the $e^+e^- \to K^+K^-$ Born cross section and charged kaon form factor using data samples at 22 c.m. energies from 2.00 to 3.08 GeV with much better precision compared to previous results. A fit of the charged kaon form factor has been performed at c.m. energy above 2.38 GeV and confirms the QCD prediction that $|F_K|$ decreases with $1/s$. The line shape of the cross section is fitted using a model based on a sum of resonances and yield a structure with a mass of $2245.6 \pm 8.3 \pm 10.8$ MeV/c^2 and a width of $136.3 \pm 11.8 \pm 9.2$ MeV, where the first uncertainties are statistical and the second ones are systematic. The nominal mass of the resonance is consistent with the $\rho(2150)$ and the $\phi(2170)$ within 2σ. However, the width deviations are more than 2σ, wider than that of the $\phi(2170)$ but narrower than that of $\rho(2150)$, and therefore further study is needed.

VIII. ACKNOWLEDGEMENT

The BESIII collaboration thanks the staff of BEPCII, the IHEP computing center and the supercomputing center of USTC for their strong support. This work is supported in part by National Key Basic Research Program of China under Contract No. 2015CB856700; National Natural Science Foundation of China (NSFC) under Contracts Nos. 11235011, 11335008, 11425524, 11625523, 11635010; the Chinese Academy of Sciences (CAS) Large-Scale Scientific Facility Program; the CAS Center for Excellence in Particle Physics (CCEPP); Joint Large-Scale Scientific Facility Funds of the NSFC and CAS under Contracts Nos. U1332201, U1532257, U1532258; CAS under Contracts Nos. KJCX2-YW-N29, KJCX2-YW-N45, QYZDJ-SSW-SLH003; 100 Talents Program of CAS; National 1000 Talents Program of China; INPAC and Shanghai Key Laboratory for Particle Physics and Cosmology; German Research Foundation DFG under Contracts Nos. Collaborative Research Center CRC 1044, FOR 2359; Istituto Nazionale di Fisica Nucleare, Italy; Koninklijke Nederlandse Akademie van Wetenschappen (KNAW) under Contract No. 530-4CDP03; Ministry of Development of Turkey under Contract No. DPT2006K-120470; National Science and Technology fund; The Swedish Resarch Council; U. S. Department of Energy under Contracts Nos. DE-FG02-05ER41374, DE-SC-0010118, DE-SC-0010504, DE-SC-0012069; University of Groningen (RuG) and the Helmholtzzentrum fuer Schwerionenforschung GmbH (GSI), Darmstadt; WCU Program of National Research Foundation of Korea under Contract No. R32-2008-000-10155-0

---

[1] C. Patrignani *et al.* (Particle Data Group), Chin. Phys. C, **40**, 100001 (2016).
[2] B. Aubert *et al.* (BABAR Collaboration), Phys. Rev. D **77**, 092002 (2008).
[3] C.P. Shen *et al.* (Belle Collaboration), Phys. Rev. D **80**, 031101(R) (2009).
[4] J.P. Lee *et al.* BABAR collaboration, Phys. Rev. D **86**, 032013 (2012).
[5] G.J. Ding *et al.*, Phy. Lett. B **650**, 390 (2007)
[6] T. Gutsche *et al.*, Phys. Rev. D **79**, 014036 (2009).
[7] S. Coito *et al.*, Phys. Rev. D **80**, 094011(2009).
[8] T.K. Pedlar *et al.*, Phys. Rev. Lett. **95**, 261803 (2005).
[9] K.S. Kamal *et al.*, Phys. Rev. Lett. **110**, 022002 (2013).
[10] D. Bisello *et al.* (DM2 Collaboration), Z. Phys. C **39**, 13 (1988).
[11] R.R. Akhmetshin *et al.* (CMD-2 Collaboration), Phys. Lett. B **669**, 217 (2008).
[12] J.P. Lees *et al.* (BaBar Collaboration), Phys. Rev. D **88**, 032013 (2013).
[13] J.P. Lees *et al.* (BaBar Collaboration), Phys. Rev. D **92**, 072008 (2015).
[14] M.R. Whalley, J. Phys. G: Nucl. Part. Phys. **29**, A1 (2003).
[15] M. Bernardini *et al.*, Phys. Lett. B **46**, 261 (1973).
[16] T.K. Pedlar *et al.* (CLEO Collaboration), Phys. Rev. Lett. **95** 261803 (2005).
[17] F.A. Harris *et al.*, Int. J. Mod. Phys. A **24**, 377 (2009).
[18] BEPCII Group, BEPCII Design Report, IHEP- Proceedings, Aug. 2001.
[19] M. Ablikim *et al.* (BESIII Collaboration), Nucl. Instrum. Meth. A **614**, 345 (2010).
[20] S. Agostinelli *et al.* (GEANT4 Collaboration), Nucl. Instrum. Meth. A **506**, 250 (2003).
[21] Z. Y. Deng *et al.*, HEP&NP **30**, 371 (2006).
[22] R.G. Ping, Chin. Phys. C, **38**(8), 083001 (2014).
[23] G. Balossini *et al.*, Nucl. Phys. B **785**, 227 (2006).
[24] B. Andersson and H. Hu, hep-ph/9810285.

TABLE II. Systematic uncertainties (%) in the measurement of the Born cross section of the $e^+e^- \to K^+K^-$ process. The total uncertainty is obtained by summing the individual contributions in quadrature.

$\sqrt{s}$ (GeV)	$\mathcal{L}$	ϵ	$1+\delta$	p	E/p	Angle	Tracking	Fit	Sig. shape	Bck. shape	Total
2.0000	0.9	0.2	0.2	0.7	0.6	0.8	0.9	0.0	0.2	0.4	1.8
2.0500	0.9	0.2	0.1	< 0.1	0.7	0.7	0.2	0.7	0.2	0.4	1.6
2.1000	0.9	0.2	0.3	0.2	0.5	0.8	0.1	0.1	0.2	0.4	1.5
2.1250	0.8	0.2	0.3	< 0.1	0.6	0.7	0.5	0.3	0.2	0.4	1.5
2.1500	0.9	0.3	0.5	< 0.1	0.6	0.7	0.5	0.1	0.3	0.4	1.5
2.1750	0.9	0.2	0.3	0.3	0.6	0.7	0.6	0.1	0.4	0.4	1.6
2.2000	0.9	0.2	0.3	0.4	0.6	0.8	0.6	0.5	0.4	0.4	1.7
2.2324	0.9	0.2	0.5	0.1	0.5	0.8	0.5	0.2	0.5	0.4	1.6
2.3094	0.9	0.2	0.2	< 0.1	0.6	0.7	0.1	0.6	0.7	0.5	1.7
2.3864	0.9	0.3	0.4	0.2	0.4	0.9	0.7	0.5	1.0	0.5	2.0
2.3960	0.9	0.3	0.4	0.3	0.4	1.0	0.8	0.4	1.0	0.6	2.1
2.5000	0.9	0.3	0.2	1.4	0.6	0.8	2.1	0.3	1.3	0.6	3.2
2.6444	0.9	0.3	0.3	0.4	0.6	0.9	1.1	2.7	1.7	0.7	3.8
2.6464	0.9	0.3	0.3	0.5	0.6	0.8	1.2	0.8	1.7	0.8	2.8
2.7000	0.9	0.3	0.3	0.5	0.4	0.9	1.5	1.0	2.0	1.2	3.3
2.8000	0.9	0.3	0.3	0.5	0.7	1.3	1.4	1.0	2.5	2.1	4.1
2.9000	0.9	0.4	0.3	0.1	0.4	0.8	1.0	1.1	3.0	3.0	4.7
2.9500	0.9	0.4	0.3	0.1	0.4	0.9	1.3	0.3	3.3	3.5	5.2
2.9810	0.9	0.4	0.3	0.5	0.5	1.2	1.6	0.2	3.4	3.8	5.6
3.0000	0.9	0.4	0.3	1.6	0.4	0.9	1.7	0.7	3.5	3.9	6.0
3.0200	0.9	0.4	0.3	1.1	0.5	0.9	1.7	0.7	3.6	4.1	6.1
3.0800	0.9	0.4	0.3	1.1	0.4	1.0	1.9	0.8	3.9	4.6	8.8

[25] S. Nova, A. Olchevski and T. Todorov (DELPHI collaboration), DELPHI 90-35 PROG 152 (1990).

[26] M. Ablikim *et al.*, (BESIII Collaboration), Chin. Pays. C, **41**(6), 063001(2017).

[27] C. Bruch *et al.*, Eur. Phys. J. C **39**, 41(2005).

[28] G.P. Lepage and S.J. Brodsky, Phys. Lett. B **87**, 359 (1979).

[29] Y. Bystritskiy *et al.*, Phys. Rev. D **72**, 114019 (2005).

[30] H. Czyz *et al.*, Eur. Phys. J. C **39**, 411 (2005).

[31] A. Hoefer *et al.*, Eur. Phys. J. C **24**, 51 (2002).

[32] W.L. Yuan *et al.*, Chin. Phys. C, **40**(2), 026201(2016).